IEEE Access
Multidisciplinary | Rapid Review | Open Access Journal

Received March 21, 2021, accepted March 28, 2021, date of publication March 31, 2021, date of current version April 9, 2021.

Digital Object Identifier 10.1109/ACCESS.2021.3070010

Harmonic Suppression and Torque Ripple Reduction of a High-Speed Permanent Magnet Spindle Motor

HAINING ZHAO, SHENBO YU, AND FENG SUN
School of Mechanical Engineering, Shenyang University of Technology, Shenyang 110870, China
Corresponding author: Haining Zhao (zhaohaining@sut.edu.cn)

This work was supported in part by the National Natural Science Foundation of China under Grant 51175350, and in part by the Scientific Research Fund Project of the Liaoning Provincial Department of Education under Grant LFGD2020002.

ABSTRACT In this paper, the method of harmonic suppression and torque ripple reduction is studied for the structure characteristics and design requirements of a high-speed permanent magnet spindle motor. According to the magnetic circuit analysis and calculation theory of the permanent magnet synchronous motor (PMSM), magnetic reluctance slots are arranged at the two ends of the rotor yoke to change the external magnetic field distribution of the permanent magnet in order to optimize the air gap magnetic density waveform. To obtain air gap flux density waveforms that are close to a sinusoidal distribution and not destroy the permanent magnet under the pre-pressure, several reluctance slots with different widths and depths arranged at two ends of the rotor yoke are used to achieve the sinusoidal distribution. Based on the selection of the pole-slot proportion, skewed-slot and a decrease in the end effect, the effects of the harmonic suppression of the harmonic electromotive force (EMF) and the reduction in the torque ripple are discussed. It is concluded that the additional loss and torque ripple of the high-speed permanent magnet spindle motor can be reduced through a reasonable design.

INDEX TERMS Permanent magnet spindle motor, torque ripple, harmonic suppression.

I. INTRODUCTION

A spindle drive system is a key component of a numerical control (NC) machine. The electric spindle has become the commonly used NC machine spindle driving system due to its superior structure and performance. The spindle motor is a core component of the electric spindle drive system. Hence, the selection of the type of the spindle motor and the its design and parameter optimization are important for improving the spindle drive system performance and accuracy [1]–[3].

The main pole magnetic field of the permanent magnet synchronous motor (PMSM) is excited by a permanent magnet, without excitation windings, leading to a decreased rotor heating. Additionally, because of its characteristics of a high efficiency and high-power density, the PMSM is particularly suitable for use in the main spindle drive system that has the requirements of high energy efficiency, and space and heat transfer. In recent decades, the research and development of the permanent magnet alternating current (AC) spindle motor has become an important research direction [4]–[7].

The ideal operation state of the PMSM is driven by the interaction between the sinusoidal stator current and sinusoidal air gap magnetic field. With the development of control technology that uses closed-loop control to make the actual current quickly follow the given value, the sine of the stator current is enough. However, due to the characteristics of the PMSM's own magnetic circuit, the no-load air gap magnetic density wave does not show a sinusoidal distribution but rather is a flat wave; this will greatly impact the performance of the motor. The waveform and size of the electromotive force (EMF) are closely related to the distribution shape and amplitude of the air gap magnetic density. To obtain a sinusoidal air gap flux density and a high-quality EMF, appropriate measures should be taken in the design and manufacturing of the motor [8]–[11].

To obtain the air gap flux density as close as possible to the sinusoidal distribution, many researchers have performed considerable research on the optimization design of the air gap flux density waveform, and achieved substantial

The associate editor coordinating the review of this manuscript and approving it for publication was Shihong Ding.

progress. The waveform of the air gap flux density can be effectively improved by using eccentric magnetic pole or magnetic pole chamfering to make the distribution of the permanent magnet exhibit an unequal thickness [12]–[19]. Although this method increases the difficulty of permanent magnet machining to a certain extent, it is easy to implement, and the wind friction will increase sharply when the uneven air gap is running at a high speed, so that it is widely used in medium- and low-speed surface-mounted permanent magnet motors. The sinusoidal waveform of the air gap magnetic field can also be obtained by changing the magnetization energy according to the sinusoidal law [15], [20], [21], by using a Halbach array structure [22]–[27], or by machining a series of modulation slots on the permanent magnet [28]. However, the magnetization and manufacturing process of the permanent magnet are more difficult, and the cost is relatively high. Using a multi-section combined pole structure, different permanent magnet materials, and different structural parameters or arrangement of some permanent magnets in a pole by a pulse width modulation method to weaken the harmonic component of the air gap magnetic field has achieved excellent results [29]–[31]. However, this approach also presents higher requirements for the rotor assembly.

The above methods have mainly focused on the shape parameters of the magnetic pole, but the high hardness, high strength and high brittleness of the permanent magnet make it very difficult to process and incur a very high cost that is the main constraint in technology application. This paper presents a design method for symmetrically setting a series of reluctance slots on the rotor yoke corresponding to both ends of the permanent magnet that can effectively suppress the main pole magnetic field and potential harmonics of the motor, greatly reducing the additional loss and pulsating torque, and at the same time, greatly reduce the difficulty of manufacturing and technological application. There have been some applications of the reluctance slot in reluctance motor that is mainly used to increase the reluctance difference between d-axis and q-axis, so as to obtain the reluctance torque caused by the reluctance difference [32]–[34]. However, the application of reluctance slot in PMSM to improve the air gap flux density waveform and suppress harmonics has been rarely reported.

For a 4-pole high-speed permanent magnet spindle motor (30000 r/min), from the perspective of the harmonic suppression of the main pole magnetic field and tooth harmonic EMF, a design scheme with a low harmonic loss and low torque ripple is obtained by a comparison of multiple schemes. These schemes provide some guidance for the design of a permanent magnet AC main spindle motor or a similar type of motor.

II. OPTIMIZATION AND CALCULATION METHOD FOR THE MAIN POLE MAGNETIC FIELD OF THE HIGH-SPEED PMSM

For protection against a tremendous centrifugal force during high-speed rotation, a layer of a high-strength non-magnetic protective sheath is placed on the outer side of the permanent magnet in the rotor design of the high-speed permanent magnet motor. A general interference fit is adopted for the permanent magnet and sheath, even if the permanent magnet has a certain pre-pressure value, which means that the permanent magnet has a value that is less than the allowable value due to tension stress.

If a permanent magnet is designed using an uneven air gap scheme, then the wedge air gap due to the eccentricity or angle of cutting will lead to some technical difficulties in the assembly of the alloy sheath. Additionally, it will be difficult to ensure the sphericity of the rotor outer surface. The air friction loss that makes a large contribution to the total loss is proportional to the cube of the motor speed, and the heterogeneity of the rotor outer surface will significantly increase the air friction loss, which is very detrimental to the spindle motor.

A. OPTIMIZATION METHOD OF THE MAIN POLE MAGNETIC FIELD

To reduce the wind friction loss between the air gap and high-speed rotating rotor, it is necessary to adopt an even air gap. For the surface-mounted PMSM with an even air gap and an equal thickness permanent magnet with parallel magnetization, the air gap magnetic density wave is a flat top wave. Assuming that the magnetic circuit saturation and the influence of the stator slot are not considered, the flux density of the air gap can be expressed as:

$$B_{\delta 0} = b_{m0}\frac{B_r}{\sigma_0} = \frac{\lambda_n B_r}{(\lambda_n + 1)\sigma_0} \tag{1}$$

where $B_{\delta 0}$ is the air gap magnetic density of no-load, b_{m0} is the no-load working point of the permanent magnet, B_r is the residual magnetic induction strength of the permanent magnet, σ_0 is the leakage factor of no-load, and λ_n is the standard value of the external magnetic permeance.

It can be concluded that the external magnetic permeance can be decreased by reducing the working point of the permanent magnet from Eq. (1), but the magnetic flux density of the air gap is reduced at the same time.

To make the air gap flux density close to a sine wave, the magnetic reluctance slot is arranged at the two ends of the rotor yoke corresponding to the permanent magnet; this arrangement increases the magnetic circuit reluctance of the permanent magnet on each side of the pole and facilitates a decrease in its external magnetic conductivity to achieve the goal of increasing the air gap magnetic sine degree. Therefore, the design of the rotor structure to achieve an approximately linear decreasing external magnetic conductivity that uses several reluctance slots with different widths and depths arranged at two ends of the rotor yoke, is shown in Figure 1.

B. FINITE ELEMENT SIMULATION AND CALCULATION

Eq. (1) describes a typical equivalent magnetic circuit analysis method. A permanent magnet is both a magnetic source and a part of the magnetic circuit. The equivalent magnetic

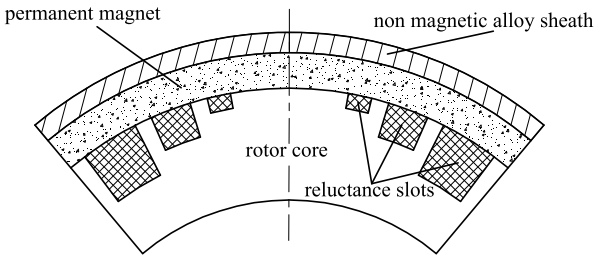

FIGURE 1. The rotor structure section.

circuit method is widely used in the initial scheme design, estimation, or scheme analogy. This method is computationally fast and is easy to analyze. The applications have been greatly restricted. The application of large-scale integrated circuits has made rapid progress in computer technology, and the application of electromagnetic field numerical analysis methods, particularly the finite element method, has become increasingly widespread.

This article builds a simulation model based on the actual parameters of a 25 kW, 4-pole spindle permanent magnet motor for which the parameters are shown in Table 1. Since the magnetic permeability of the ferromagnetic material is much larger than that of air and the magnetic density of the stator core yoke has not reached the saturation state, the stator punch is selected, and the circle is the first type of the homogeneous boundary. The permanent magnets are magnetized in parallel. The mesh division at the air gap is reasonably encrypted. The radial gap and circumferential segmentation are used to manually control the air gap. The grid size can render a more accurate calculation result. To facilitate the subsequent harmonic analysis, the number of circumferential segments is 1024, the number of model units is 8374, and the number of the air gap units is 5032, accounting for 60% of the total. This size not only guarantees the accuracy of the calculation results but also controls the calculation time and ensures the feasibility of the calculation. The calculated magnetic field distribution and the magnetic density distributions with and without considering the cogging effect are shown in Figure 2.

TABLE 1. Parameters of the 25kW PMSM prototype.

Parameters	Value	Parameters	Value
Rated power	25kW	Stator core outer diameter	125mm
Pole number	4	Stator core inner diameter	82mm
Rated voltage	273V	Rated current	58A
Air gap length	3mm	Frequency	1000Hz
Axial length	130mm	Thickness of the PM	4.5mm

Figure 3 shows a comparison of the air gap magnetic flux density waveform with and without reluctance slots. The air gap flux density waveform is improved to some extent with the reluctance slots. Therefore, by optimizing the position,

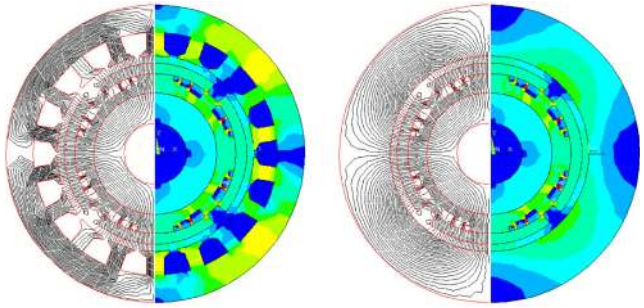

(a) with slot effect (b) without slot effect

FIGURE 2. Magnetic field distribution and magnetic density distribution.

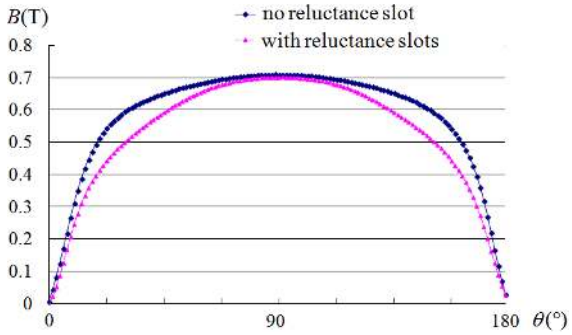

FIGURE 3. Comparison of the air gap flux density waveform.

span and depth of the reluctance slots, a distribution of the air gap flux density that is close to sinusoidal can be obtained.

C. HARMONIC ANALYSIS AND PARAMETER OPTIMIZATION

The impact of reluctance slots on the air gap flux density harmonics can be analyzed by the Fourier analysis of the waveform data obtained from different structures. Figure 4 shows the comparison of the harmonics analysis results where the air gap magnetic field contains rich harmonics when the reluctance slot is arranged at two ends of the rotor yoke (such as that shown in Figure 1).

Although a slight decrease in the amplitude of the fundamental wave is observed, the harmonic is greatly weakened, which is clearly highly beneficial for enhancing the performance of the motor.

Many methods can be used to measure the sinusoidal characteristics of the waveforms. In addition to some parameters that reflect the content of a certain harmonic, the parameters that focus on the overall performance of the harmonics, such as the total harmonic distortion (THD) and total harmonic factor (THF), are of more concern. Because the THD is more intuitive than the fundamental root mean square (RMS) value, it is most commonly used in engineering applications. However, this method also takes into account the harmonic with integer times of 3 in the three-phase symmetrical windings, that is the disadvantage of this method.

The sinusoidity of the air gap flux density waveform is evaluated by calculating the root mean square of the ratio

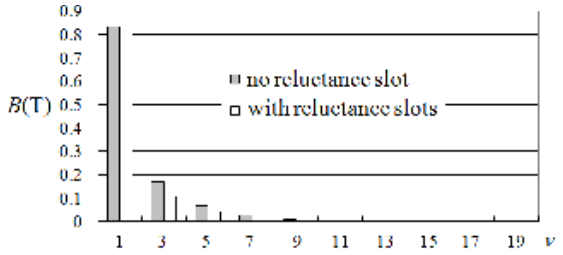

FIGURE 4. Contrast diagram of the harmonic analysis.

between the harmonic components G_n and the fundamental component G_1 which are not greater than a certain order n, that is, the total harmonic distortion rate. The total harmonic distortion rate THD can be calculated according to Eq. (2). Because a harmonic amplitude of more than 20 is quite small and has relatively little impact on the performance of the motor, in this paper, only the harmonics of less than 20 are considered.

$$THD = \sqrt{\sum_{n=2}^{H} \left(\frac{G_n}{G_1}\right)^2} \times 100\% \tag{2}$$

Figure 5 shows the distribution of the reluctance slots at the two ends of the rotor yoke, where α_{PM} is the permanent magnet pole arc angle, $\theta_{r1}, \theta_{r2}, \theta_{r3} \ldots \theta_{rn}$ are the 1st, 2nd, 3rd and so on spans from the two ends to the middle, respectively, and $h_{r1}, h_{r2}, h_{r3} \ldots h_{rn}$ are the 1st, 2nd, 3rd and so on depths of the reluctance slots from the two ends to the middle, respectively. All of the tooth spans between the two reluctance slots are 2 degrees considering the process requirements.

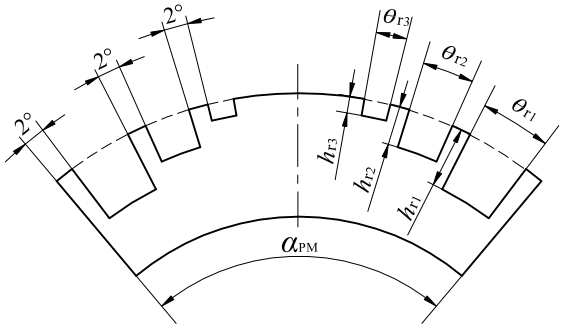

FIGURE 5. The rotor core and magnetic reluctance slot.

We compare the sinusoidal waveform of the air gap magnetic density with different structure sizes. According to the analysis and calculation of the fundamental amplitude and the THD rate of the magnetic density of the air gap, the scheme with best comprehensive performance is chosen as the rotor structure of the motor. The structure sizes and calculation results of the different schemes are shown in Table 2.

An examination of the data presented in the Table shows that the position, span and depth of the reluctance slot have strong influence on the total harmonic distortion rate of the air gap flux density waveform. The THD of the air gap flux density waveform can be greatly reduced by opening the reluctance slots.

TABLE 2. Contrast of the THD with different structures.

α_{PM} (°)	θ_{rn} (°)	h_{rn} (mm)	THD (%)
90	0	0	24.37
90	8,5,2	3,2,1	15.79
90	10,7,4	4,3,2	9.65
90	10,7,4	6,4,2	8.32
85	0	0	22.29
85	8,5,2	3,2,1	14.68
85	10,7,4	4,3,2	7.43
85	10,7,4	6,4,2	6.36
80	0	0	21.78
80	8,5,2	3,2,1	14.26
80	10,7,4	4,3,2	7.38
80	10,7,4	6,4,2	6.13
75	0	0	21.64
75	8,5,2	3,2,1	14.17
75	10,7,4	4,3,2	7.15
75	10,7,4	6,4,2	6.02
70	0	0	22.41
70	8,5,2	3,2,1	14.79
70	10,7,4	4,3,2	7.42
70	10,7,4	6,4,2	6.24

The position and span of the reluctance slot are related, and this relationship determines the harmonic suppression effect to a large extent. When the span of the slot is constant, the harmonic suppression effect will be very limited when the depth increases to a certain value. The magnetic load will be reduced as a function of the decrease in the pole arc length in the permanent magnet. To ensure the power performance of the motor when other parameters are unchanged, the electrical load should increase, but the stator space is limited and the electric density of the stator is bounded. Therefore, to ensure the running safety of the motor and meet the cooling requirements, it is necessary to consider the actual situation.

The scheme selected in this paper is that the pole arc angle is 80°, the slot spans are 10°, 7° and 4°, and the slot depths are 6, 4 and 2 mm, respectively. Under these conditions, the total harmonic distortion rate of air gap flux density waveform is 6.13%.

III. HARMONIC SUPPRESSION OF THE TOOTH HARMONIC EMF AND REDUCTION IN THE TORQUE RIPPLE

A slotted stator produced the air gap magnetic conductivity and the tooth harmonic EMF; the EMF waveform was saw-tooth-like. The motor loss is increased and the torque ripple is produced; the harm is even more obvious for the spindle motor with high-speed rotation. Therefore, it is necessary to weaken the tooth harmonic EMF.

A. SELECTION OF THE POLE-SLOT PROPORTION

The pole-slot proportion is an important factor that affects the additional loss, additional torque and vibration and noise characteristics of the PMSM. Therefore, the motor with high performance requirements should be considered carefully.

The tooth harmonic EMF of the integral slot can be reduced by short-pitch winding or distributed winding. Figure 6 shows a comparison of the harmonic fundamental amplitude ratio between the different pole-slot proportion and different spans, where z is the number of stator slots, $2p$ is the number of poles, and y_1 is the number of the slots of the winding span. The 24-4-5 scheme shows a good suppression of each harmonic and can be used as the first choice for the integral slot scheme of the motor.

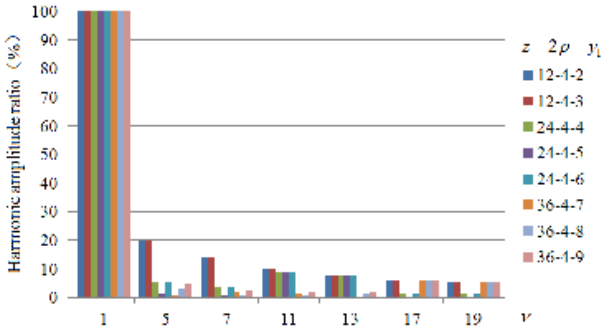

FIGURE 6. Harmonic distribution of the integral slot.

Because the winding coefficient of the tooth harmonic EMF is exactly equal to the winding coefficient of the fundamental wave, the tooth harmonic EMF in each coil group is directly superimposed due to the same phase. Therefore, there will be strong tooth harmonic in the phase EMF for the integral slot. The fundamental wave EMF will also be reduced by the same ratio if the tooth harmonic EMF is reduced through short-pitch winding or distributed winding [35], [36].

The tooth harmonic EMF of each coil group has a certain phase offset due to the asymmetrical distribution of the fractional slot winding. A partial offset exists for the tooth harmonic EMFs of each coil group with respect to each other with the superposition of the vector overlay; thus, it has a very good suppression effect on the tooth harmonic EMF. However, the fractional slot winding is used to make the harmonic distribution more abundant than the integer slot winding that have odd harmonics [27], [37]–[40]. For 4-pole motors, a large number of sub-harmonics exist for 9, 15, 21, 27, etc. stator slots. Figure 7 shows a comparison of the harmonic fundamental amplitude ratio with the slot-pole ratios of 6/4, 18/4 and 36/4. Additionally, it can be more convenient to use short-pitch winding or distributed winding to suppress the harmonic by increasing the number of slots. In this case, the number of windings is increased, and since the manufacture of windings is more complex, the technological performance of the motor becomes poor. Therefore, the selection of the pole-slot proportion should be considered based on the motor size and process conditions.

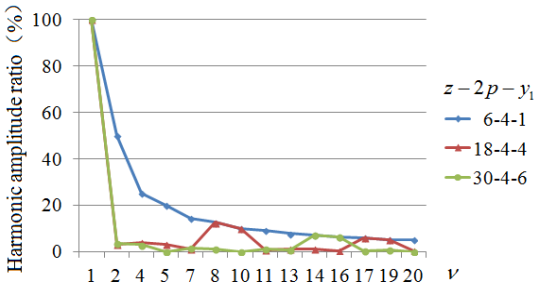

FIGURE 7. Harmonic distribution of the fractional slot.

B. INFLUENCE OF THE SKEWED-SLOT ON THE HARMONIC EMF AND TORQUE RIPPLE WEAKENING

The skewed-slot process is another effective method for suppressing the tooth harmonic EMF and weakening the torque ripple. The tooth harmonic EMF of each point in the axial direction has a certain offset in the same phase when the slot skew is accepted, greatly decreasing the tooth harmonic contribution in the total EMF. Then, the torque ripple caused by the additional torque can be reduced. This effect plays a highly important role in improving the torque stability of the permanent magnet motor at a low speed [31], [41], [42].

For the permanent magnet motor, due to the limitations in permanent magnet processing, the rotor segmented inclined pole or stator skewed-slot is generally used. The process of the rotor segmented inclined pole is complex and the torque ripple weakening effect is relatively poor, so that the stator skewed-slot method is adopted in this paper.

Figure 8 shows the torque ripple distribution under a pair of poles when the motor is in a straight slot, skewed half slot and skewed one slot. It is observed that the skewed-slot can greatly reduce the torque ripple. The torque ripple coefficient K can be calculated according to Eq. (3).

$$K = \frac{T_{\max} - T_{\min}}{T_{\max} + T_{\min}} \times 100\% \tag{3}$$

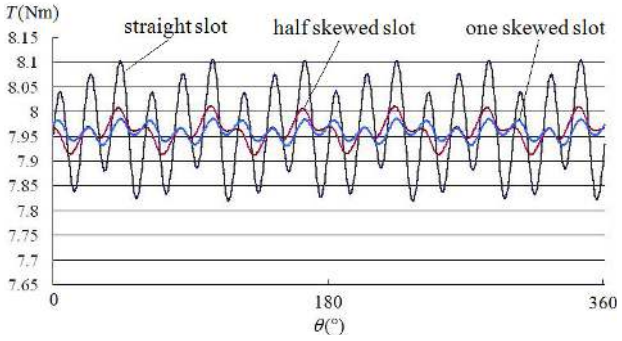

FIGURE 8. Effect of the process of the skewed-slot on the torque ripple.

The calculation shows that the torque ripple coefficient K is 3.39% when the motor is in the straight slot. The torque ripple of the skewed half slot and skewed one slot were reduced to 1.26% and 0.5%, and their decline rates were

62.9% and 85.1%, respectively. The effect of torque ripple weakening was apparent.

C. INFLUENCE OF THE END EFFECT ON THE TORQUE RIPPLE

An edge magnetic field is present near the two ends of the motor core, making the axial distribution of the air gap flux density uneven; that is, an end effect exists. When the lengths of the stator and rotor are equal, a small part of the rotor flux will enter the stator core from the end face of the stator due to the end effect. The distribution of the flux is shown in Figure 9(a).

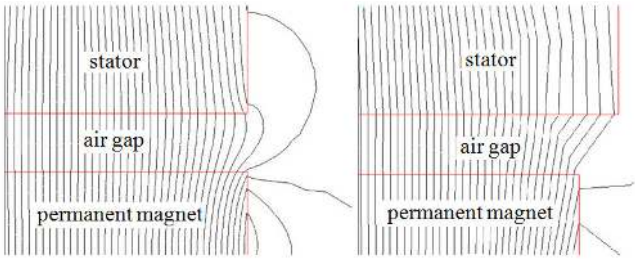

FIGURE 9. The end effects.

In some cases, to improve the utilization of materials, the rotor core length is significantly longer than the stator core, and the end effect of the air gap magnetic field is significantly increased. However, due to a change in the stator end face cogging permeance, a certain torque fluctuation will be produced. For the motor with a high torque fluctuation index, the design of a stator core length that is slightly larger than the rotor core length can largely solve this problem. The distribution of the magnetic line of force is shown in Figure 9(b).

By calculating and comparing the end effects of the four different specifications of surface-mounted permanent magnet motors, the relationship between the end flux ϕ_d entering the stator core from the end face of the stator and the ratio of the length of the stator core exceeding the length of the rotor core l_z to the length of the air gap l_g is obtained, as shown in Figure 10.

It is observed that when l_z/l_g approaches 1, the end face of the stator that enters the flux of the stator core ϕ_d is very close to 0. That is, almost the entire main pole flux enters the stator core through the air gap, and the torque ripple caused by the end effect is almost completely eliminated.

IV. PROTOTYPE MANUFACTURING AND EXPERIMENTAL ANALYSIS

To verify the effectiveness of the proposed harmonic suppression and torque ripple reduction methods for high-speed permanent magnet spindle motors, a prototype is manufactured and the related performance indicators are tested, as shown in Figure 11. The measured current waveform, back

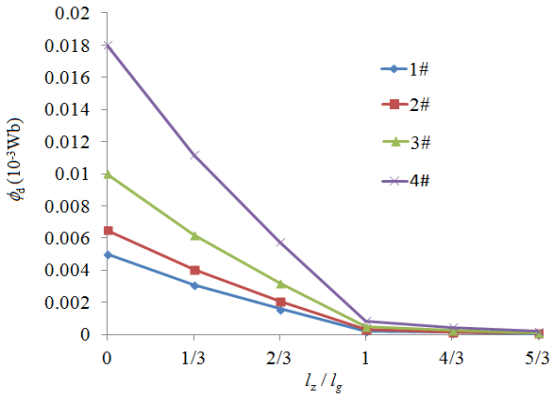

FIGURE 10. Effect of the extended length of the stator core on the end magnetic flux.

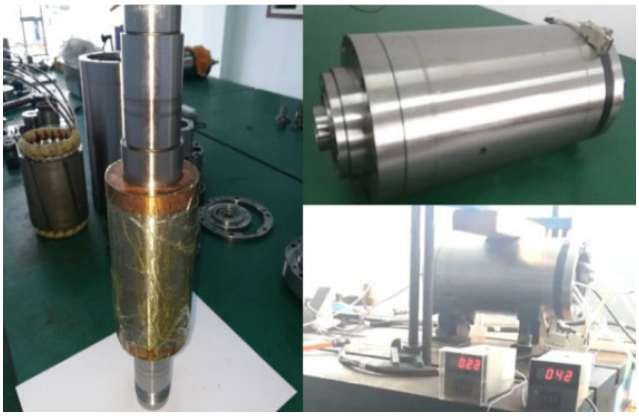

FIGURE 11. Prototype and test.

EMF waveform and corresponding harmonic analyses are shown in Figures 12 and 13.

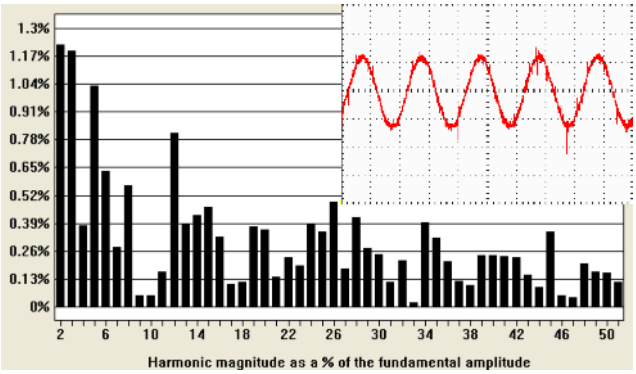

FIGURE 12. Measured current waveform and corresponding harmonic analysis.

The type test under the rated state is carried out on a high-speed spindle motor test bench. Due to the lack of torque and speed sensor suitable for the high-speed spindle permanent magnet motor in this paper, the test is carried out by the method of the mechanical back-to-back test. The prototype is used as the tested motor, and a spindle permanent magnet

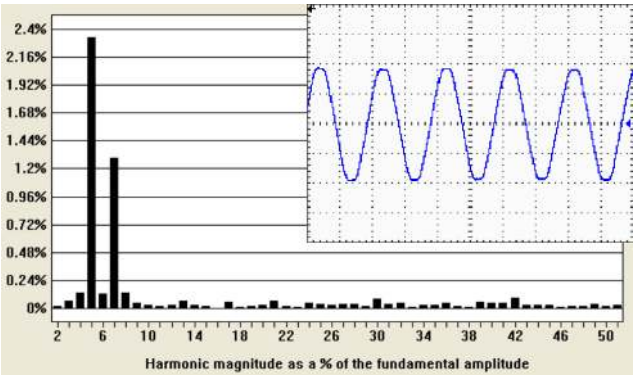

FIGURE 13. Measured back EMF waveform and corresponding harmonic analysis.

motor with the same parameters is used as the generator. When the average value of the input power of the tested motor and the output power of the generator are 25kW, the difference between them is approximately considered to be their common loss, and then a part of the power index of the tested motor is obtained.

The measured data and calculated values are compared in Table 3. The difference between the measured efficiency and power factor values and the calculated values are quite small. Although some errors are obtained, the effectiveness of the design is verified to a certain extent. The THD of the measured current waveform is 2.091%, the THD of the measured back EMF waveform is 2.679%, and the harmonic weakening effect is also obvious.

TABLE 3. Comparison of the measured data and calculated values.

	Efficiency %	Power factor	Current THD, %	EMF THD, %
Calculated value	91.55	0.986	2.060	2.650
Measured value	91.65	0.990	2.091	2.679
Deviation, %	0.11	0.40	1.48	1.08

V. CONCLUSION

In this paper, based on the structural characteristics of a high-speed motor, a new type of structure is proposed. The sinusoidal distributed air gap magnetic density is obtained by setting reluctance slots on the rotor yoke corresponding to both ends of the permanent magnet. The processing technology is relatively simple, and the reliable operation of the permanent magnet is ensured. The position, span and depth of the reluctance slot strongly influence the total harmonic distortion rate of the air gap flux density waveform. The THD of the air gap flux density waveform can be greatly reduced by opening the magnetoresistance slot. In this paper, the THD of the air gap flux density waveform is reduced to 6.13% when the reluctance slot is set reasonably. The prototype is manufactured, and a simple test is carried out. Compared with the experimental and numerical results, the deviation of THD from the measured current waveform and EMF are 1.48% and 1.08%, respectively, verifying the effectiveness of the method. Due to the lack of torque and a speed sensor suitable for high-speed spindle permanent magnet motor in this paper, only a rough test is carried out. Some errors are present due to the lack of consideration of the difference of the additional loss between the tested motor and the accompanying motor. In the future research work, it is necessary to further test and separate the losses, and carry out a more in-depth analysis.

REFERENCES

[1] D. Gerada, A. Mebarki, N. L. Brown, C. Gerada, A. Cavagnino, and A. Boglietti, "High-speed electrical machines: Technologies, trends, and developments," *IEEE Trans. Ind. Electron.*, vol. 61, no. 6, pp. 2946–2959, Jun. 2014.

[2] W. Purwanto, T. Sugiarto, H. Maksum, D. Putra, and E. Alwi, "Comparison of three topologies rotor to improve efficiency and torque for high-speed spindle motor applications," in *Proc. ICAITI*, Sep. 2018, pp. 176–181.

[3] S. J. Sung, G. H. Jang, J. W. Jang, J. Y. Song, and H. J. Lee, "Vibration and noise in a HDD spindle motor arising from the axial UMF ripple," *IEEE Trans. Magn.*, vol. 49, no. 6, pp. 2489–2494, Jun. 2013.

[4] H. A. A. Awan, T. Tuovinen, S. E. Saarakkala, and M. Hinkkanen, "Discrete-time observer design for sensorless synchronous motor drives," *IEEE Trans. Ind. Appl.*, vol. 52, no. 5, pp. 3968–3979, Sep. 2016.

[5] O. Ocak, M. Onsal, and M. Aydin, "Development of a 7.5kW high speed interior permanent magnet synchronous spindle motor for CNC milling machine," in *Proc. ICEM*, Sep. 2018, pp. 704–709, doi: 10.1109/ICELMACH.2018.8506701.

[6] J. Shen, X. Qin, and Y. Wang, "High-speed permanent magnet electrical machines—Applications, key issues and challenges," *CES Trans. Electr. Mach. Syst.*, vol. 2, no. 1, pp. 23–33, Mar. 2018.

[7] F. Zhang, G. Du, T. Wang, F. Wang, W. Cao, and J. L. Kirtley, "Electromagnetic design and loss calculations of a 1.12-MW high-speed permanent-magnet motor for compressor applications," *IEEE Trans. Energy Convers.*, vol. 31, no. 1, pp. 132–140, Mar. 2016.

[8] Q. Sun, Z. Deng, and Z. Zhang, "Analytical calculation of rotor eddy current losses in high-speed permanent magnet machines accounting for influence of slot opening," *Trans. China Electrotech. Soc.*, vol. 33, no. 9, pp. 1994–2004, May 2018.

[9] A. E. Hoffer, I. Petrov, J. J. Pyrhonen, J. A. Tapia, and G. Bramerdorfer, "Analysis of a tooth-coil winding permanent-magnet synchronous machine with an unequal teeth width," *IEEE Access*, vol. 8, pp. 71512–71524, 2020.

[10] Y. L. Xu, Q. Z. Li, and T. Wang, "Optimal design of no-load air gap flux density of permanent magnet synchronous motor," *J. Southwest Jiaotong Univ.*, vol. 44, no. 4, pp. 513–516, Aug. 2009.

[11] X. H. Lu and J. H. Liang, "Air gap magnetic field analysis of surface-mounted permanent magnet motors," *Electr. Mach. Control*, vol. 15, no. 7, pp. 15–19, Jul. 2011.

[12] H. Kim and J. Moon, "Improved rotor structures for increasing flux per pole of permanent magnet synchronous motor," *IET Electr. Power Appl.*, vol. 12, no. 3, pp. 415–422, Mar. 2018.

[13] Z. Y. Yu, Y. Li, Y. T. Jing, J. M. Du, and Z. C. Wang, "No-Load characteristic analysis of surface-mounted permanent magnet synchronous motor with non-concentric pole based on hybrid magnetic field analysis method," *Trans. China Electrotech. Soc.*, vol. 35, no. 18, pp. 3811–3820, Sep. 2020.

[14] W. Chen, J. Ma, G. Wu, and Y. Fang, "Torque ripple reduction of a salient-pole permanent magnet synchronous machine with an advanced step-skewed rotor design," *IEEE Access*, vol. 8, pp. 118989–118999, 2020, doi: 10.1109/ACCESS.2020.3005762.

[15] Z. Chen, C. Xia, Q. Geng, and Y. Yan, "Modeling and analyzing of surface-mounted permanent-magnet synchronous machines with optimized magnetic pole shape," *IEEE Trans. Magn.*, vol. 50, no. 11, pp. 1–4, Nov. 2014, doi: 10.1109/TMAG.2014.2327138.

[16] P. Hu, D. Wang, S. Jin, Y. Wei, C. Chen, N. Lin, Q. Zhang, X. Wu, H. Zhu, and F. Sun, "The modified model of third-harmonic shaping for a surface-mounted permanent-magnet synchronous motor under parallel magnetization," *IEEE Trans. Ind. Appl.*, vol. 56, no. 5, pp. 4847–4856, Sep. 2020, doi: 10.1109/TIA.2020.3008369.

[17] Z. Yu, Y. Li, Y. Jing, J. Du, and Z. Wang, "Analytical model for magnetic field calculation of SPMSM with chamfered pole considering iron core saturation," *IET Electr. Power Appl.*, vol. 14, no. 10, pp. 1856–1864, Oct. 2020, doi: 10.1049/iet-epa.2019.1013.

[18] A. Rahideh and T. Korakianitis, "Analytical magnetic field distribution of slotless brushless permanent magnet motors Part I. Armature reaction field, inductance and rotor eddy current loss calculations," *IET Electr. Power Appl.*, vol. 6, no. 9, pp. 628–638, Nov. 2012.
[19] C. Zhou, G. Yang, and J. Su, "PWM strategy with minimum harmonic distortion for dual three-phase permanent-magnet synchronous motor drives operating in the overmodulation region," *IEEE Trans. Power Electron.*, vol. 31, no. 2, pp. 1367–1380, Feb. 2016.
[20] G. X. Zhao, Y. Zhang, H. Y. Ge, Y. Liu, and B. D. Bai, "Prediction of flux density distribution in permanent magnet motor with eccentric magnetic pole," *Electr. Mach. Control*, vol. 24, no. 6, pp. 24–32, Jun. 2020, doi: 10.15938/j.emc.2020.06.004.
[21] Z. H. He, "Pole optimization design of bread-loaf eccentric magnetic pole permanent magnet motor," *Micro Motors*, vol. 53, no. 8, pp. 27–32, Aug. 2020.
[22] S. Dwari and L. Parsa, "Design of Halbach-array-based permanent-magnet motors with high acceleration," *IEEE Trans. Ind. Electron.*, vol. 58, no. 9, pp. 3768–3775, Sep. 2011.
[23] R. P. Praveen, M. H. Ravichandran, V. T. S. Achari, V. P. J. Raj, G. Madhu, and G. R. Bindu, "A novel slotless Halbach-array permanent-magnet brushless DC motor for spacecraft applications," *IEEE Trans. Ind. Electron.*, vol. 59, no. 9, pp. 3553–3560, Sep. 2012.
[24] S. Sadeghi and L. Parsa, "Multiobjective design optimization of five-phase Halbach array permanent-magnet machine," *IEEE Trans. Magn.*, vol. 47, no. 6, pp. 1658–1666, Jun. 2011.
[25] S. Zhang, W. Zhang, J. Zhao, and R. Wang, "Multi-objective optimization design and analysis of double-layer winding Halbach fault-tolerant motor," *IEEE Access*, vol. 9, pp. 3725–3734, 2021, doi: 10.1109/ACCESS.2020.3047860.
[26] T. Zhang, X. Ye, L. Mo, and Q. Lu, "Electromagnetic performance analysis on the bearingless permanent magnet synchronous motor with Halbach magnetized rotor," *IEEE Access*, vol. 7, pp. 121265–121274, 2019.
[27] S. F. Jia, D. L. Liang, and Z. Q. Zhu, "Enhanced flux modulation of FSCW consequent pole PM machine employing stator slot Halbach PM," in *Proc. ICEM*, Aug. 2020, pp. 1985–1991, doi: 10.1109/ACCESS.2019.2937897.
[28] W. Chai and B.-I. Kwon, "A magnetic pole modulation method on surface permanent magnet machines for high performances with different magnetization," *IEEE Access*, vol. 7, pp. 79839–79849, 2019, doi: 10.1109/ACCESS.2019.2923449.
[29] Y. B. Yang, X. H. Wang, and C. Q. Zhu, "Research of modular pole on the reduction of torque ripple of permanent magnet synchronous motor," *Electr. Mach. Control*, vol. 17, no. 2, pp. 34–38, Feb. 2013, doi: 10.15938/j.emc.2013.02.009.
[30] S. Chaithongsuk, N. Takorabet, and F. Meibody-Tabar, "On the use of pulse width modulation method for the elimination of flux density harmonics in the air-gap of surface PM motors," *IEEE Trans. Magn.*, vol. 45, no. 3, pp. 1736–1739, Mar. 2009.
[31] D. Wang, X. Wang, and S.-Y. Jung, "Cogging torque minimization and torque ripple suppression in surface-mounted permanent magnet synchronous machines using different magnet widths," *IEEE Trans. Magn.*, vol. 49, no. 5, pp. 2295–2298, May 2013.
[32] L. Jing, J. Cheng, and T. Ben, "Analytical method for magnetic field and electromagnetic performances in switched reluctance machines," *J. Electr. Eng. Technol.*, vol. 14, no. 4, pp. 1625–1635, Apr. 2019, doi: 10.1007/s42835-019-00167-0.
[33] L. Gargalis, V. Madonna, P. Giangrande, R. Rocca, M. Hardy, I. Ashcroft, M. Galea, and R. Hague, "Additive manufacturing and testing of a soft magnetic rotor for a switched reluctance motor," *IEEE Access*, vol. 8, pp. 206982–206991, 2020.
[34] Y. Zhu, H. Wu, and J. Zhang, "Regenerative braking control strategy for electric vehicles based on optimization of switched reluctance generator drive system," *IEEE Access*, vol. 8, pp. 76671–76682, 2020, doi: 10.1109/ACCESS.2020.2990349.
[35] S. Niu, T. Sheng, X. Zhao, and X. Zhang, "Operation principle and torque component quantification of short-pitched flux-bidirectional-modulation machine," *IEEE Access*, vol. 7, pp. 136676–136685, 2019, doi: 10.1109/ACCESS.2019.2942482.
[36] Y. Chen, W. Hao, Y. Yang, L. Kang, and Q. Zhang, "Winding and electromagnetic analysis for 39-slot/12-pole frameless permanent magnet synchronous motor," in *Proc. 22nd Int. Conf. Electr. Mach. Syst. (ICEMS)*, Aug. 2019, pp. 1–6.
[37] A. M. EL-Refaie, "Fractional-slot concentrated-windings synchronous permanent magnet machines: Opportunities and challenges," *IEEE Trans. Ind. Electron.*, vol. 57, no. 1, pp. 107–121, Jan. 2010.
[38] K. Wang and H. Lin, "A novel 24-slot/10-pole dual three-phase fractional-slot overlapped winding for low non-working space harmonics and stator modularization," *IEEE Access*, vol. 8, pp. 85490–85503, 2020, doi: 10.1109/ACCESS.2020.2992258.
[39] E. Carraro, N. Bianchi, S. Zhang, and M. Koch, "Design and performance comparison of fractional slot concentrated winding spoke type synchronous motors with different slot-pole combinations," *IEEE Trans. Ind. Appl.*, vol. 54, no. 3, pp. 2276–2284, May 2018.
[40] Z. Q. Zhu, Z. P. Xia, L. J. Wu, and G. W. Jewell, "Analytical modeling and finite-element computation of radial vibration force in fractional-slot permanent-magnet brushless machines," *IEEE Trans. Ind. Appl.*, vol. 46, no. 5, pp. 1908–1918, Oct. 2010.
[41] X. Ge, Z. Q. Zhu, G. Kemp, D. Moule, and C. Williams, "Optimal step-skew methods for cogging torque reduction accounting for three-dimensional effect of interior permanent magnet machines," *IEEE Trans. Energy Convers.*, vol. 32, no. 1, pp. 222–232, Mar. 2017.
[42] E. S. Obe, "Calculation of inductances and torque of an axially laminated synchronous reluctance motor," *IET Electr. Power Appl.*, vol. 4, no. 9, pp. 783–792, Nov. 2010.

HAINING ZHAO was born in Hengshui, China, in 1981. He received the B.S. and M.S. degrees from the Shenyang University of Technology, in 2003 and 2009, respectively.

He is currently an Engineer with the School of Mechanical Engineering, Shenyang University of Technology. His current research interests include mechanical and electrical coupling, CNC machine tool dynamic characteristics, noise and vibration suppression of PMSM, and rotor dynamic characteristics.

SHENBO YU was born in Shenyang, China, in 1956. He received the B.E. degree in water pump from the Shenyang Institute of Mechanical and Electrical Engineering, Shenyang, in 1982, and the M.E. degree in mechanical engineering and the Ph.D. degree in electrical engineering from the Shenyang University of Technology, Shenyang, in 1988 and 2006, respectively.

He is currently a Professor with the School of Mechanical Engineering, Shenyang University of Technology. His current research interests include mechanical and electrical coupling, CNC machine tool dynamic characteristics, noise and vibration suppression of PMSM, rotor dynamic characteristics, and low noise fan design.

FENG SUN was born in Fuxin, China, in 1978. He received the B.S. and M.S. degrees from the Shenyang University of Technology, China, in 2002 and 2005, respectively, and the Ph.D. degree from the Kochi University of Technology, in 2010.

He is currently a Professor with the School of Mechanical Engineering, Shenyang University of Technology. His current research interests include magnetic suspension technology and NC machining technology and equipment.